# SOLID-STATE NUCLEAR MAGNETIC RESONANCE OF $^{133}$Cs IN CsPbBr$_3$+Bi SEMICONDUCTOR PEROVSKITES

**A. N. Gavrilenko,[a,]*** **O. I. Gnezdilov,[b]** **A. V. Emeline,[c]**    UDC 539.143.43
**A. V. Shurukhina,[c]** **E. V. Schmidt,[a]** **A. F. Ivanov,[a]** **and V. L. Matukhin[a]**

*$^{133}$Cs NMR was employed to study the structural characteristics and properties of perovskites at the atomic level. CsBi$_x$Pb$_{1-x}$Br$_3$ perovskites doped with Bi at concentrations of 0.0059, 0.0072, and 0.0120 were studied. The importance of high-quality materials for applications in optics and photonics was noted. $^{133}$Cs NMR showed high sensitivity for studying these concentrations of Bi, which affect the stability of perovskites and their dynamic parameters.*

**Keywords:** *nuclear magnetic resonance, perovskites, method sensitivity, solar energy conversion, semi-conductor materials.*

**Introduction.** Photovoltaics or direct conversion of solar energy into electrical energy is one of the most promising renewable energy sources. The development of solar energy in the XXIst century remains at the forefront of all alternative sources. Perovskite-halide solar cells with a solar-energy conversion efficiency of >20% are a new and promising class of solar cells that are currently being thoroughly studied [1]. Special attention is being paid to lead halide perovskites (LHPs) such as CsPbX$_3$ because of their desirable optical properties and better ecological stability than hybrid organic-inorganic perovskite halides [2, 3]. CsPbX$_3$ materials can be used in LEDs [4], photomultipliers [5], memory devices [6], radiation sensors [7], and others because of their electrical and optical properties, e.g., tunable band gap over the whole visible region, high optical absorption coefficients, long service life, high electron and hole mobility, and resistance to defects. Therefore, further improvement of the functional properties is the main goal of both basic and applied research on CsPbX$_3$ materials. Heterovalent doping is a classical method for modifying the electronic and optical properties of semiconductor materials and is easily applied to CsPbX$_3$ perovskites [8]. The dopant Bi could replace Pb atoms by stable and controlled methods owing to the similar ionic radii of Pb$^{2+}$ and Bi$^{3+}$ (1.19 and 1.03 Å) [9, 10]. Doping with Bi could increase the efficiency of solar cells by increasing the absorption of visible light [11]. It also allows interfacial charge transfer of LHPs and other materials to be accurately controlled by energy-level alignment [12]. The effect of doping on the physical properties of LHPs is still not fully understood, despite the broad interest in doping with Bi. This could prevent optimization of the doping conditions in various applications.

The crystal structure of perovskites is described by the formula ABX$_3$, where A and B are cations and X is an anion. The Cs atoms in CsPbBr$_3$ occupy one set of structural positions with *m*-symmetry. The closest environment around the Cs atoms consists of eight Pb atoms in the B positions (A = Cs):
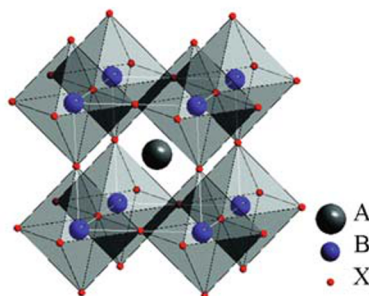
*To whom correspondence should be addressed.

[a]Kazan State Power Engineering University, Kazan, Russia; email: ang_2000@mail.ru; [b]Kazan (Volga Region) Federal University, Kazan, Russia; [c]St. Petersburg State University, St. Petersburg, Russia. Translated from Zhurnal Prikladnoi Spektroskopii, Vol. 90, No. 4, pp. 577–583, July−August, 2023. Original article submitted March 3, 2023.

One method for displaying this structure has the larger cation A surrounded by 12 anions in cuboctahedral coordination and B cations surrounded by six anions in octahedral coordination. The X anions are surrounded by two B cations and four A cations. The probability of forming the perovskite structure is determined by the ratio of the ionic radii of the starting atoms. Let us calculate the Goldschmidt tolerance factor $t$ and octahedral coefficient $\mu$ to estimate this probability:

$$t = (R_A + R_X)[\sqrt{2}\,(R_B + R_X)], \quad \mu = R_B/R_X\,, \tag{1}$$

where $R_A$, $R_B$, and $R_X$ are ionic radii of atoms A, B, and X. These coefficients for the perovskite structure should fall in the limits $0.825 < t < 1.059$ and $0.414 < \mu < 0.732$ [13].

The main structural blocks of inorganic perovskite frameworks are [PbX6/2] octahedra connected by vertices along three orthogonal spatial directions. Electronic states of the halide and lead form a valence band and conductivity band. Thus, controlled doping in the Pb position in the octahedra can affect such fundamental properties as the position of the Fermi level, conductivity type, and lifetime and mobility of charge carriers, which provides an important advantage for optoelectronic devices with electron transfer [14–16]. Heterovalent doping by $Bi^{3+}$ ions was shown to lead to a shift of the Fermi level into the conductivity band, strong absorption at wavelengths exceeding the wavelength of the corresponding band gap energy, and a change of conductivity to *n*-type [17, 18].

Several radiospectroscopic methods, including electron paramagnetic resonance (EPR), nuclear quadrupole resonance (NQR), and nuclear magnetic resonance (NMR) have been used to study the properties of semiconductor materials on the atomic level [19, 20].

$^{133}$Cs NMR has been used to study chemical shifts of nuclei, the anisotropy of chemical shielding, quadrupole tensor parameters, and the relationship of these characteristics to the nuclear environment in various compounds [21–25]. NMR methods could be used to obtain useful information on the material characteristics, intermolecular interactions, and properties that affect the stability of perovskites and their dynamic parameters [26, 27].

The aim of the present work was to study polycrystals of perovskite CsPbBr$_3$+Bi using solid-state $^{133}$Cs NMR.

**Experimental.** Doping with Bi in the Pb position in CsPbBr$_3$ was studied using wet chemical synthesis of three samples of CsBi$_x$Pb$_{1-x}$Br$_3$ ($x = 0.0059$, 0.0072, and 0.0120) and pure CsPbBr$_3$. The tolerance factor $t$ for the selected samples was calculated using Eq. 1 before the syntheses to estimate the possibility of forming the perovskite crystal structure. The obtained values were within the required limits. The calculated and weighed masses of the starting components (CsBr, PbBr$_2$, BiBr$_3$) were dissolved in HBr solution. The salts dissolved completely at 160$^{\circ}$C. Then, the obtained solutions were evaporated to produce dry powders. The phase composition of the samples was monitored using x-ray diffraction (XRD) analysis. The XRD analysis was performed in the resource center for x-ray structure studies at St. Petersburg State University on a Bruker Discover D8 x-ray diffractometer.

NMR experiments used a Bruker Avance III WB 400 NMR spectrometer ($B = 9.4$ T) equipped with a 4-mm probe with double resonance and the capability for magic-angle spinning (MAS). MAS NMR spectra were obtained for samples with naturally abundant $^{133}$Cs using a onepulseq-experiment with $\pi/8$ pulses of duration 2.5 $\mu$s, a 1-s delay before the next cycle, and spinning frequency 9 kHz. CsNO$_3$ in D$_2$O was used as the reference compound to measure the chemical shifts. The number of accumulations was 2048. NMR spectra of $^{133}$Cs nuclei without spinning were obtained using a solidecho-experiment.

**Results and Discussion.** $^{133}$Cs is an ideal nucleus for solid-state NMR studies because it is 100% abundant in nature, has a relatively small quadrupole moment $Q = -0.00343 \cdot 10^{-28}$ m$^2$, possesses nuclear spin quantum number $I = 7/2$, and demonstrates a remarkable range of chemical shifts of ~600 ppm. $^{133}$Cs NMR is very sensitive to the local medium of Cs and can detect fine differences in the local Cs bonding that are unresolved by diffraction studies. Many applications of solid-state $^{133}$Cs NMR for a broad spectrum of chemical compounds have been reported [27–30]. The experimental details of the procedure for synthesizing Bi-doped CsPbBr$_3$ and data from XRD analysis, scanning electron microscopy, x-ray photoelectron spectroscopy, and diffuse reflectance spectroscopy have been published [31].

Let us briefly discuss the theory and important parameters [32], i.e., the isotropic chemical shift ($\delta_{iso}$), anisotropic information of the chemical shift as an interval ($\Delta\delta$), asymmetry of the chemical shift $\eta_\delta$, and nuclear quadrupole coupling constants ($C_Q$) and its asymmetry parameter ($\eta_Q$). According to the commonly accepted Haeberlen convention:

$$\delta_{iso} = \frac{1}{3}\,(\delta_{xx} + \delta_{yy} + \delta_{zz})\,, \quad \Delta\delta = \delta_{zz} - \delta_{iso}\,, \quad \eta_\delta = \frac{\delta_{yy} - \delta_{xx}}{\Delta\delta}\,, \quad 0 \leq \eta_\delta \leq 1\,. \tag{2}$$
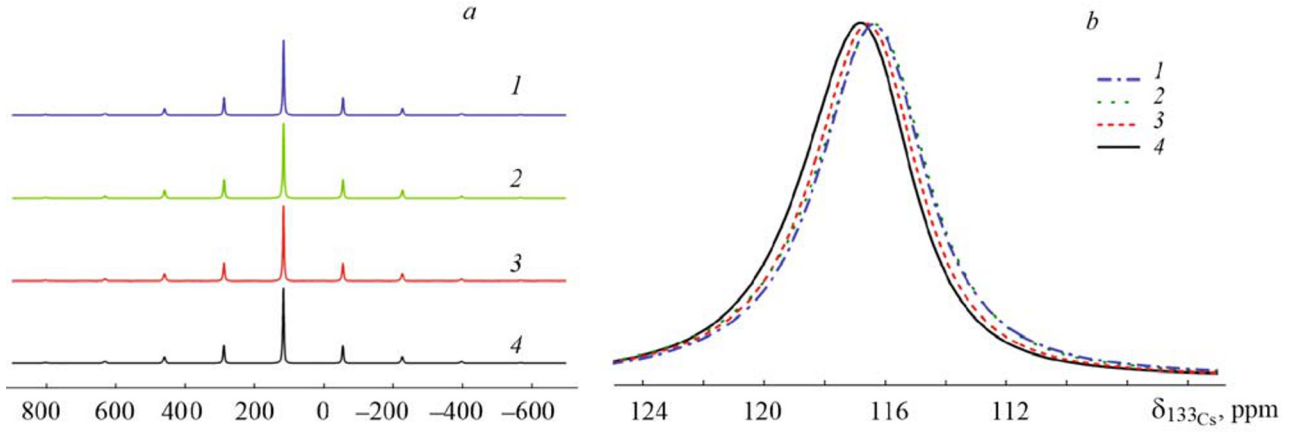
Fig. 1. MAS $^{133}$Cs NMR spectra for CsBi$_x$Pb$_{1-x}$Br$_3$ with Bi concentrations $x = 0.0120$ (1), 0.0072 (2), 0.0059 (3), and 0.0000 (4) at 9.4 T with spinning frequency 9 kHz (a) and their chemical shifts (b).

TABLE 1. Parameters of MAS $^{133}$Cs NMR Spectra of Bi-Doped CsPbBr$_3$ Compounds

| Bi concentration, % | Chemical shift $\delta_{iso}$, ppm | $\eta_Q$ | $C_Q$, kHz | Lorentz broadening, Hz |
|---|---|---|---|---|
| 0.00 | 117.170 | 0.011 | 195 | 202.96 |
| 0.59 | 116.941 | 0.012 | 195 | 205.54 |
| 0.72 | 116.665 | 0.010 | 202 | 215.30 |
| 1.20 | 116.660 | 0.010 | 194 | 206.60 |

In this instance, the eigen values of the chemical shift $\{\delta_{xx}, \delta_{yy}, \delta_{zz}\}$ are ordered:

$$|\delta_{yy} - \delta_{iso}| \leq |\delta_{xx} - \delta_{iso}| \leq |\delta_{zz} - \delta_{iso}| . \tag{3}$$

The eigen values of the electric field gradient (EFG) tensor $\{V_{xx}, V_{yy}, V_{zz}\}$ are ordered according to the relationship $V_{xx} \leq V_{yy} \leq V_{zz}$. The quadrupole constant $C_Q$ and asymmetry parameter $\eta_Q$ are related to the EFG tensor eigen values by:

$$C_Q = \frac{eQV_{zz}}{h} , \quad \eta_Q = \frac{V_{yy} - V_{xx}}{V_{zz}} , \tag{4}$$

where $e$ is the elementary charge and $h$, Boltzmann's constant. The orientation of the EFG tensor relative to the main axes of the shielding tensor is described by Euler angles $\{\alpha, \beta, \gamma\}$ in terms of the ROS convention.

The isotope $^{133}$Cs has a relatively small quadrupole moment and low gyromagnetic ratio. MAS $^{133}$Cs NMR spectra were recorded for all four samples at the corresponding field sweeps. Figure 1 shows MAS $^{133}$Cs NMR spectra at room temperature and their chemical shifts.

The Cs atoms occupy one set of structural positions in CsPbBr$_3$ with $m$-symmetry while the closest environment around the Cs atoms consists of eight Pb atoms located in the B positions. In this case, the MAS $^{133}$Cs NMR spectrum agreed fully with this structure [29] and had chemical shift $\delta(^{133}\text{Cs}) \approx 117.17$ ppm with width 203 Hz (Fig. 1a). The set of satellite lines in the MAS $^{133}$Cs NMR spectrum corresponded to the noncubic symmetry of the Cs crystallographic positions [29]. The parameters of the MAS $^{133}$Cs NMR spectra of CsPbBr$_3$ doped with Bi were calculated using the TopSpin 3.1 and QUEST programs [33, 34]. Table 1 presents the modeling results. Estimates of the quadrupole coupling constant $C_Q$ gave values in the range 194–202 kHz with asymmetry parameter $\eta_Q = 0.011$. The best overlap in these models was close to 89% for each spectrum. Figure 2 shows the modeled spectrum and experimental MAS $^{133}$Cs NMR spectrum (undoped
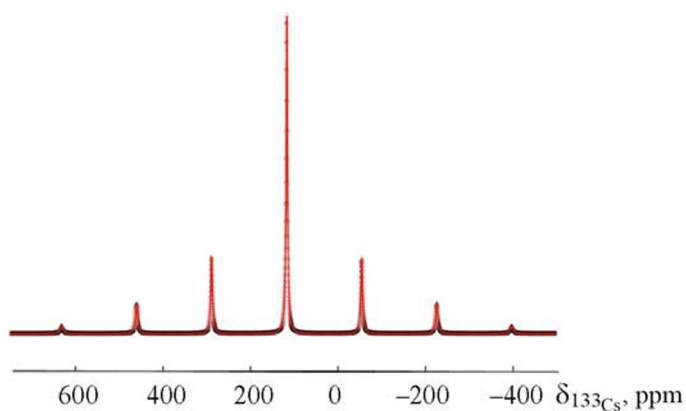
Fig. 2. Experimental (points) and modeled (line) MAS $^{133}$Cs NMR spectra for CsPbBr$_3$ at 9.4 T with spinning frequency 9 kHz; Table 1 presents the modeling parameters for the undoped sample.
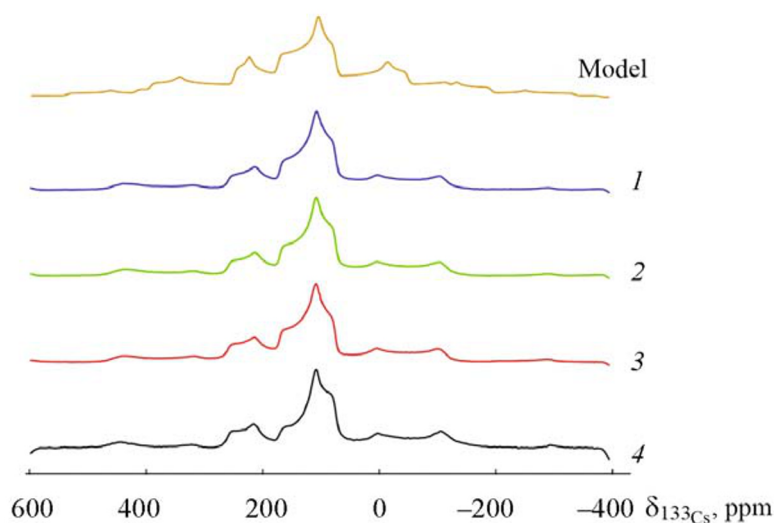


Fig. 3. Static $^{133}$Cs NMR spectra of CsBi$_x$Pb$_{1-x}$Br$_3$ at 9.4 T for $x$ = 0.0120 (1), 0.0072 (2), 0.0059 (3), and 0.0000 (4); model parameters $C_Q$ = 195 kHz, $\eta_Q$ = 0.01, $\delta_{iso}$ = 117 ppm, $\Delta\delta$ = 57 ppm, $\alpha = 0^o$, $\beta = 30^o$, $\gamma = 0^o$.

CsPbBr$_3$, chemical shift $\delta_{iso}$ = 117.170 ppm, $\eta_Q$ = 0.011, $C_Q$ = 195 kHz, Lorentz broadening 202.96 Hz, spinning frequency 9 kHz). The obtained parameters of the MAS $^{133}$Cs NMR spectrum practically coincided with the literature data. MAS $^{133}$Cs NMR spectra of doped CsPbBr$_3$+Bi samples at 9.4 T also showed a set of satellite lines. However, the peaks of the resonance lines for the central transition (1/2 ↔ −1/2) in the doped samples was shifted slightly lower and covered the range 117.17–116.6 ppm (Fig. 1b). It is noteworthy that narrow resonance lines also persisted in spectra of the doped samples. Thus, the results for MAS $^{133}$Cs NMR spectra of CsPbBr$_3$+Bi indicated that doping with Bi was effective and that Bi atoms were regularly incorporated into the CsPbBr$_3$ crystal lattice.

The anisotropy of chemical shift $\Delta\delta$ was estimated from measured static $^{133}$Cs NMR spectra (Fig. 3). The value $\Delta\delta$ = 56.6 ± 0.3 ppm was obtained from the results of processing the four spectra. A model of the static spectrum was built based on the anisotropy estimated by us (Fig. 3 gives the model parameters) and the parameters previously determined from results of our MAS $^{133}$Cs NMR experiments with an undoped sample (Table 1).

**Conclusions.** Perovskites doped with Bi, i.e., $CsBi_xPb_{1-x}Br_3$ ($x$ = 0.0059, 0.0072, and 0.0120) and pure $CsPbBr_3$ were synthesized by a wet chemical method. MAS $^{133}Cs$ NMR spectra were obtained for these polycrystalline samples. Processing of the experimental MAS $^{133}Cs$ NMR spectra using the TopSpin program produced the hyperfine coupling parameters in the studied $CsPbBr_3$+Bi compounds. The estimated quadrupole coupling constant $C_Q$ = 196.5 kHz (average of four spectra); asymmetry parameter $\eta_Q$ = 0.011. The anisotropy of the chemical shift was estimated from measured static $^{133}Cs$ NMR spectra and was ~56.6 ppm. Chemical shifts were obtained for MAS $^{133}Cs$ NMR spectra of doped $CsPbBr_3$ + Bi and undoped samples. Peaks of resonance lines for the central transition (1/2 ↔ −1/2) in doped samples were shifted slightly lower and covered the range 117.17–116.66 ppm. The chemical shift decreased smoothly with increasing Bi dopant concentration. In this case, the line width at half height remained practically unchanged. The small shift of the spectral line could be explained by a change of electron distribution near the resonant nuclei that resulted from doping the starting compound. The studies of the $^{133}Cs$ NMR spectra indicated that Bi doping was effective, i.e., the dopant was regularly incorporated into the crystal lattice of $CsPbBr_3$+Bi.

# REFERENCES

1. A. V. Dmitriev and I. P. Zvyagin, *Phys. — Usp.*, **53**, No. 8, 789–803 (2010).
2. E. I. Marchenko, S. A. Fateev, A. A. Petrov, E. A. Goodilin, and A. B. Tarasov, *Mendeleev Commun.*, **30**, 279–281 (2020); doi: 10.1016/j.mencom.2020.05.005.
3. Z.-J. Li, E. Hofman, A. H. Davis, A. Khammang, J. T. Wright, B. Dzikovski, R. W. Meulenberg, and W. Zheng, *Chem. Mater.*, **30**, 6400–6409 (2018); doi: 10.1021/acs.chemmater.8b02657.
4. S. A. Veldhuis, P. P. Boix, N. Yantara, M. Li, T. C. Sum, N. Mathews, and S. G. Mhaisalkar, *Adv. Mater.*, **28**, Article ID 6804 (2016).
5. Y. Li, Z.-F. Shi, S. Li, L.-Z. Lei, H.-F. Ji, D. Wu, T.-T. Xu, Y.-T. Tian, and X.-J. Li, *J. Mater. Chem. C*, **5**, 8355–8360 (2017); doi: 10.1039/C7TC02137B.
6. A. Kostopoulou, E. Kymakis, and E. Stratakis, *J. Mater. Chem. A*, **6**, 9765–9798 (2018); doi: 10.1039/C8TA01964A.
7. V. B. Mykhaylyk, H. Kraus, V. Kapustianyk, H. J. Kim, P. Mercere, M. Rudko, P. Da Silva, O. Antonyak, and M. Dendebera, *Sci. Rep.*, **10**, 8601 (2020); doi: 10.1038/s41598-020-65672-z.
8. B. Luo, F. Li, K. Xu, Y. Guo, Y. Liu, Z. Xia, and J. Z. Zhang, *J. Mater. Chem. C*, **7**, No. 10, 2781–2808 (2019).
9. X. L. Miao, T. Qiu, S. F. Zhang, H. Ma, Y. Q. Hu, F. Bai, and Z. C. Wu, *J. Mater. Chem. C*, **5**, No. 20, 4931–4939 (2017); doi: 10.1039/C7TC00417F.
10. J. Yin, G. H. Ahmed, O. M. Bakr, J. L. Bredas, and O. F. Mohammed, *ACS Energy Lett.*, **4**, No. 3, 789–795 (2019); doi: 10.1021/acsenergylett.9b00209.
11. M. Saliba, T. Matsui, J. Y. Seo, K. Domanski, J. P. Correa-Baena, M. K. Nazeeruddin, S. M. Zakeeruddin, W. Tress, A. Abate, A. Hagfeldt, and M. Gratzel, *Energy Environ. Sci.*, **9**, No. 6, 1989–1997 (2016); doi: 10.1039/c5ee03874j.
12. R. Begum, M. R. Parida, A. L. Abdelhady, B. Murali, N. M. Alyami, G. H. Ahmed, M. N. Hedhili, O. M. Bakr, and O. F. Mohammed, *J. Am. Chem. Soc.*, **139**, No. 2, 731–737 (2017); doi: 10.1021/jacs.6b09575.
13. C. J. Bartel, C. Sutton, B. R. Goldsmith, R. Ouyang, C. B. Musgrave, L. M. Ghiringhelli, and M. Scheffler, *Sci. Adv.*, **5**, eaav0693 (2019); doi: 10.1126/sciadv.aav0693.
14. L. Xu, S. Yuan, H. Zeng, and J. Song, *Mater. Today Nano*, **6**, 100036 (2019); doi: 10.1016/j.mtnano.2019.100036.
15. R. Begum, M. R. Parida, A. L. Abdelhady, B. Murali, N. M. Alyami, G. H. Ahmed, M. N. Hedhili, O. M. Bakr, and O. F. Mohammed, *J. Am. Chem. Soc.*, **139**, 731–737 (2017); doi: 10.1021/jacs.6b09575.
16. O. A. Lozhkina, A. A. Murashkina, V. V. Shilovskikh, Y. V. Kapitonov, V. K. Ryabchuk, A. V. Emeline, and T. Miyasaka, *J. Phys. Chem. Lett.*, **9**, 5408–5411 (2018); doi: 10.1021/acs.jpclett.8b02178.
17. A. L. Abdelhady, M. I. Saidaminov, B. Murali, V. Adinolfi, O. Voznyy, K. Katsiev, E. Alarousu, R. Comin, I. Dursun, L. Sinatra, E. H. Sargent, O. F. Mohammed, and O. M. Bakr, *J. Phys. Chem. Lett.*, **7**, No. 2, 295–301 (2016); doi: 10.1021/acs.jpclett.5b02681.
18. F. Aiello and S. Masi, *Nanomaterials*, **11**, No. 8, 2024 (2021); doi: 10.3390/nano11082024.
19. V. V. Ogloblichev, V. L. Matukhin, I. Y. Arapova, E. V. Schmidt, and R. R. Khusnutdinov, *Appl. Magn. Res.*, **50**, 619–625 (2019); doi: 10.1007/s00723-018-1096-9.

20. V. L. Matukhin, A. N. Gavrilenko, E. V. Schmidt, S. B. Orlinskii, I. G. Sevastianov, S. O. Garkavyi, J. Navratil, and P. Novak, *Appl. Magn. Res.*, **52**, 1729–1737 (2021); doi: 10.1007/s00723-021-01409-z.

21. J. Skibsted, T. Vosegaard, H. Bildsoe, and H. J. Jakobsen, *J. Phys. Chem.*, **100**, 14872–14881 (1996); doi: 10.1021/jp9608741.

22. T. Minami, Y. Tokuda, H. Masai, Y. Ueda, Y. Ono, S. Fujimura, and T. Yoko, *J. Asian Ceram. Soc.*, **2**, 333–338 (2014); doi: 10.1016/j.jascer.2014.07.001.

23. S. Kroeker, K. Eichele, R. E. Wasylishen, and J. F. Britten, *J. Phys. Chem. B*, **101**, 3727–3733 (1997); doi: 10.1021/jp970043a.

24. O. B. Lapina, V. M. Mastikhin, A. A. Shubin, K. M. Eriksen, and R. Fehrmann, *J. Mol. Catal. A: Chem.*, **99**, No. 2, 123–130 (1995); doi: 10.1016/1381-1169(95)00043-7.

25. O. B. Lapina, V. V. Terskikh, A. A. Shubin, V. M. Mastikhin, K. M. Eriksen, and R. Fehrmann, *J. Phys. Chem. B*, **101**, No. 45, 9188–9194 (1997); doi: 10.1021/jp971789b.

26. L. Piveteau, V. Morad, and M. V. Kovalenko, *J. Am. Chem. Soc.*, **142**, 19413–19437 (2020); doi: 10.1021/jacs.0c07338.

27. A. Karmakar, A. Bhattacharya, D. Sarkar, G. M. Bernard, A. Mar, and V. Michaelis, *Chem. Sci.*, **12**, 3253–3263 (2021); doi: 10.1039/d0sc05614f.

28. F. Ji, F. Wang, L. Kobera, S. Abbrent, J. Brus, W. Ning, and F. Gao, *Chem. Sci.*, **12**, 1730–1735 (2021); doi: 10.1039/d0sc05264g.

29. A. Karmakar, A. Bhattacharya, G. M. Bernard, A. Mar, and V. K. Michaelis, *ACS Mater. Lett.*, **3**, 261–267 (2021); doi: 10.1021/acsmaterialslett.0c00596.

30. Y. Chen, S. R. Smock, A. H. Flintgruber, F. A. Perras, R. L. Brutchey, and A. J. Rossini, *J. Am. Chem. Soc.*, **142**, No. 13, 6117–6127 (2020); doi: 10.1021/jacs.9b13396.

31. I. M. Sharaf, A. V. Shurukhina, I. S. Komarova, and A. V. Emeline, *Mendeleev Commun.*, **31**, 465–468 (2021); doi: 10.1016/j.mencom.2021.07.009.

32. V. I. Chizik, Yu. S. Chernyshev, A. V. Donets, V. V. Frolov, A. I. Komolkin, and M. G. Shelyapina, *Magnetic Resonance and its Applications*, XX, Springer, Cham, Heidelberg, New York, Dordrecht, London (2014), doi: 10.1007/978-3-319-05299-1.

33. Bruker TopSpin; https://www.bruker.com/service/information-communication/user-manuals/nmr.htm.

34. F. A. Perras, C. M. Widdifield, and D. L. Bryce, *Solid State Nucl. Magn. Reson.*, **45**–**46**, 36–44 (2012); doi: 10.1016/j.ssnmr.2012.05.002.